



Tutorial: simulating a rod pinch diode for pulsed radiography with Trak and GamBet

Stanley Humphries, Copyright 2010

Field Precision

PO Box 13595, Albuquerque, NM 87192 U.S.A.

Telephone: +1-505-220-3975

Fax: +1-617-752-9077

E mail: techinfo@fieldp.com

Internet: <http://www.fieldp.com>

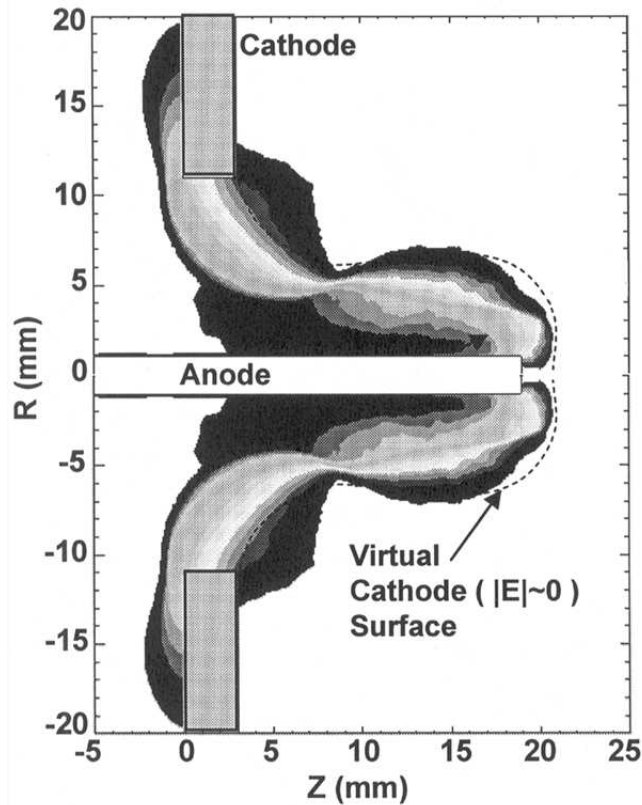


Figure 1: **LSP** simulation of a generic rod pinch diode. Applied voltage: 4.1 MV, total current: 78 kA, collected electron current: 58 kA. (Courtesy of S. Swanekamp.)

The calculations described in this report demonstrate the ability of **Trak** to represent complex particle dynamics in pinched-beam diodes and confirm the accuracy of **GamBet** for dose predictions. I compared results to detailed PIC simulations and experiments described in Ref. [1] and [2]. Figure 1 shows **LSP** results for the first example, a generic rod-pinch diode. The PIC code has been run to equilibrium conditions at an applied voltage of 4.1 MV. The cathode at ground potential is a 3.0 mm thick plate with an aperture of radius 11.0 mm. The cylindrical anode at high voltage has radius 1.0 mm and extends 15.0 mm past the downstream cathode face. Figure 1 shows the electron flow patterns calculated with **LSP** and the approximate shape of the virtual cathode (*i.e.*, the surface where $|\mathbf{E}|$ approaches zero). The predicted total current is 78 kA and the electron current that arrives at the anode is 58 kA.

In contrast to **LSP**, **Trak** is a ray-tracing code that seeks a self-consistent equilibrium directly. The method involves tracing particle orbits to determine their contribution to space-charge and current density. The fields are

updated and particle orbits retraced. The process is repeated for several cycles to achieve self-consistent convergence. The rod-pinch presents a significant challenge because of the complex, non-laminar electron orbits and the dominant role of beam-generated fields. **Trak** has several unique features to facilitate pinched-beam models:

- The beam-generated magnetic field is calculated on the same conformal mesh used for the electric field.
- The code accepts multiple emission surfaces with different particle species.
- For efficient models of electron-ion counterflow, the time step is adjusted to reflect the particle mass.
- Boundary currents are assigned to electrodes based on particle capture.
- Adjustable field averaging gives improved convergence.

Figure 2 shows the geometry of the **Trak** simulation. (For comparisons to the **LSP** results, note that the z direction is reversed and that **Trak** creates r - z plots). The geometry is the same as that of Fig. 1 except that I used rounded edges on the cathode and anode to make it easier to assign emission surfaces. The solution volume covers the axial range $-50.0 \text{ mm} \leq z \leq 50.0 \text{ mm}$ and the radial range $0.0 \text{ mm} \leq r \leq 50.0 \text{ mm}$. The left boundary and radial outer boundary are set to ground potential, while the potential of the anode is 4.1 MV. The figure shows electrostatic equipotential lines for the self-consistent solution and trajectories for every tenth electron (blue) and ion (red). A space-charge-limited flux of protons leaves the anode surface from the tip to a point 10.0 mm upstream of the cathode face. The range ensures contribution of ion space-charge over the region accessible to electrons. Note that the choice of ion species has negligible effect on the steady-state solution and the run time.

A space-charge-limited flux of electrons is emitted from a portion of the cathode. The emission surface extends to a radius of 20.0 mm on the upstream side and 13.75 mm on the downstream side. I observed convergence problems in previous rod-pinch simulations described in Ref. [3]. In the present calculations, I found that a careful choice of the range of the electron emission surface greatly reduces variations of emitted current between cycles. Figure 3 illustrates some considerations:

- On the upstream face of cathode, electrons emitted at a radius greater than 14.0 mm are reabsorbed. I included a set of these electrons because they affect the emission conditions for the electrons created at smaller

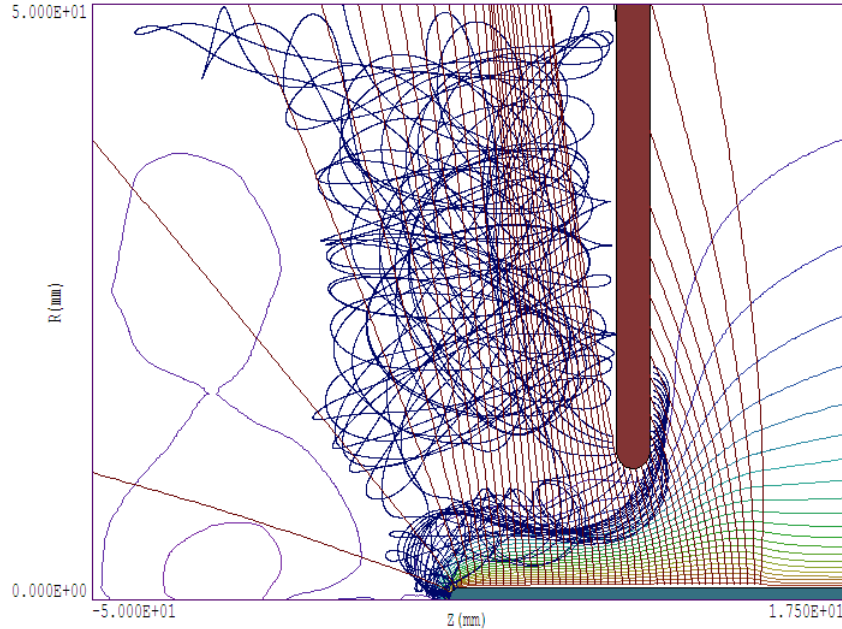


Figure 2: Generic rod pinch. Equipotential lines of the self-consistent electric field with electron orbits (blue) and ion orbits (red). Every tenth orbit plotted.

radius that reach the anode. An implication is that the emitted electron current will be higher than the current of electrons that cross the gap. Extending the outer emission radius past 20.0 mm would accomplish nothing but extending the run time.

- On the downstream face, electrons produced at radius $r > 12.5$ do not travel directly to the anode. Instead, they follow complex drift orbits in the low-field space. Because of the reduced electric field on downstream face, these electrons carry only a small fraction of the gap current but consume a large portion of the run time. Also, their emission properties are sensitive to small variations in the solution. I found that the radius choice of 13.75 mm represented the effect of downstream electrons without wasting code resources.

Figure 4 shows the convergence history of total emitted current. After initially large excursions representing relaxation of the electric field near the emission surfaces, there is a slow rise to an equilibrium value with relatively small variations. Convergence is aided by new form of the **Trak** beam-averaging command:

```
Avg = 0.10 (20 0.025)
```

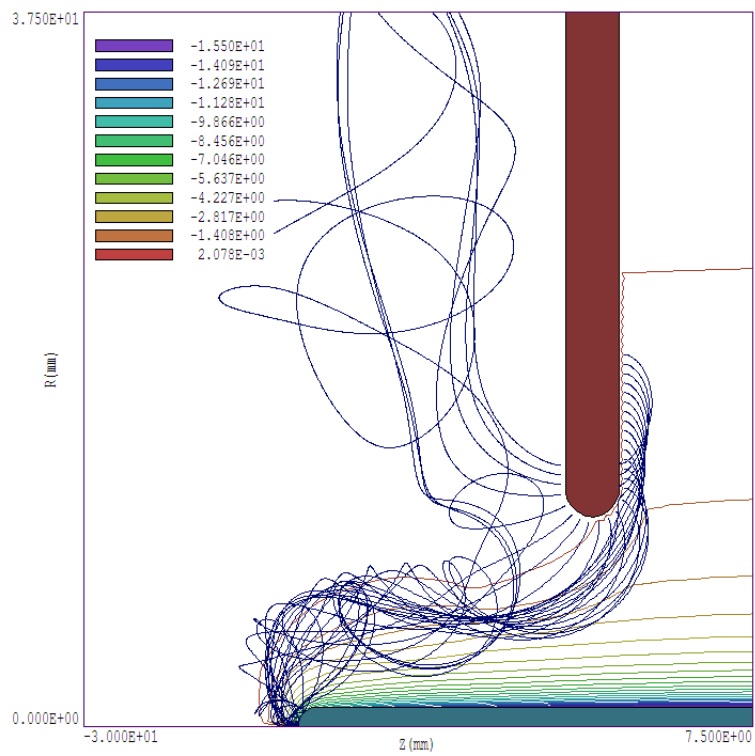


Figure 3: Generic rod pinch. Detail of electron orbits showing contour lines of $|B_\theta|$. Every tenth orbit plotted.

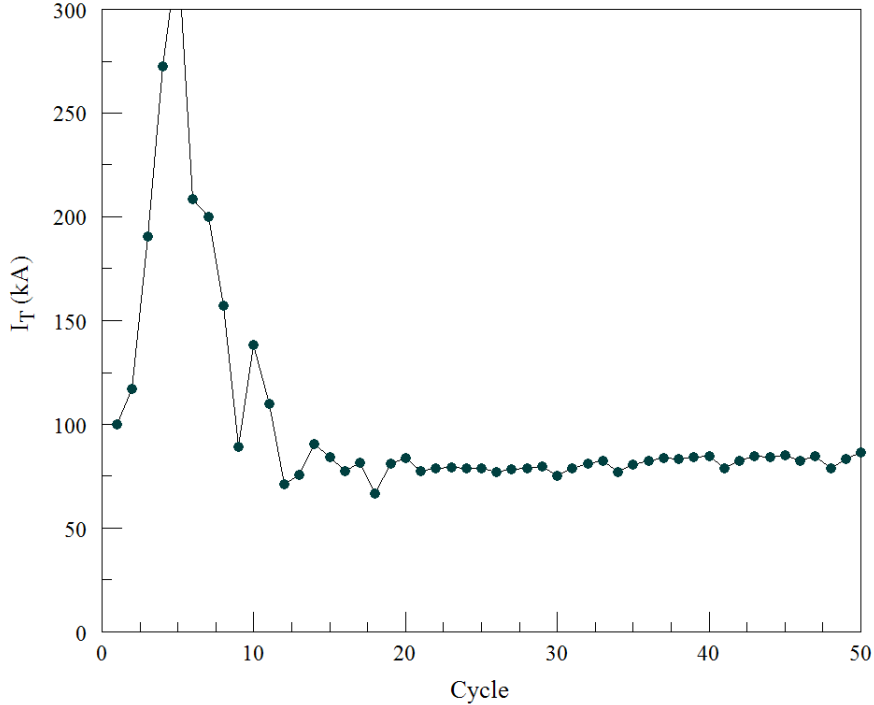


Figure 4: Generic rod pinch. Total emitted current versus cycle number.

The beam-averaging factor α determines how the space-charge and current calculated on the present cycle are combined with information from previous cycles. If ρ_c is the space-charge density calculated from the present orbits, then the space-charge density is adjusted according to:

$$\rho^{n+1} = (1 - \alpha)\rho^n + \alpha\rho_c. \quad (1)$$

The implication is that the charge and current density are averaged over approximately $1/\alpha$ cycles. The command shown sets $\alpha = 0.10$ over cycles 1 through 20 for a quick approach to an equilibrium solution, and then sets $\alpha = 0.025$ to reduce variations in cycles 21 through 50.

Using values at cycle 45 for comparison to the **LSP** results, **Trak** predicts 63.09 kA of emitted electron current and 18.84 kA of ion current. While all ions cross the gap, some electrons are reabsorbed by the cathode. Therefore, the actual electron current is determined by measuring electrons collected at the anode. I loaded the output **PRT** file into **GenDist** and set the filter $r \leq 1.5$ mm. The result is a collected electron current of 58.33 kA, giving a total current of 77.2 kA. Both the electron and ion current values are within 1% of the **LSP** prediction. For comparison to the torodial field data in Fig. 3, the predicted value of B_θ on the anode surface is 15.43 tesla. To conclude discussion of this calculation, Fig. 5 plots $|\mathbf{E}|$ for comparison to the virtual

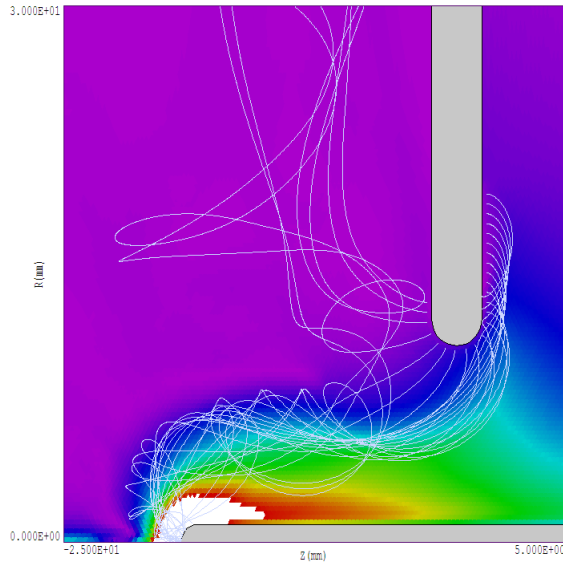


Figure 5: Generic rod pinch. Selected electron orbits and color-coding by $|\mathbf{E}|$ to show the virtual cathode surface.

cathode surface in Fig. 1.

The second example is an end-to-end calculation of radiation generation in the Asterix experiments described in Ref. [1] and [2]. Figure 6 shows the baseline geometry. The anode is a 1.0 mm radius tungsten rod that extends 16.0 mm past the downstream face of the cathode. The references describe the anode as *tapered*. In the absence of exact dimensions, I used a rounded tip. As in the previous calculation, the cathode is a 3 mm thick plate with an aperture of radius 11.0 mm. The downstream vacuum chamber is an aluminum hemisphere of inner radius 100.0 mm and thickness 10.0 mm. Because of evolving capabilities of the Monte Carlo engine in **LSP**, the calculations reported Ref. [1] and [2] used a combination of numerical and analytic techniques. My calculations were done entirely with the numerical capabilities of **Trak** and **GamBet**.

The first step is to simulate the rod-pinch diode with **Trak**, using a procedure similar to the previous example. The applied voltage is 5.8 MV. The total emitted current averaged over cycles 40 through 50 is 122.28 kA \pm 4.74 kA and the ion current is 30.33 kA. The electron current that reaches the anode is 83.82 kA, giving a total gap current of 114.2 kA. The **Trak** script contains a command calling for a recording of information on the final electric field along with values of B_θ . Figure 7a shows measured values for the diode on the Asterix accelerator. Both the **LSP** and **Trak** results are in good agreement with the measured current near the peak voltage.

The **Trak** calculation generates an output PRT (particle) file containing

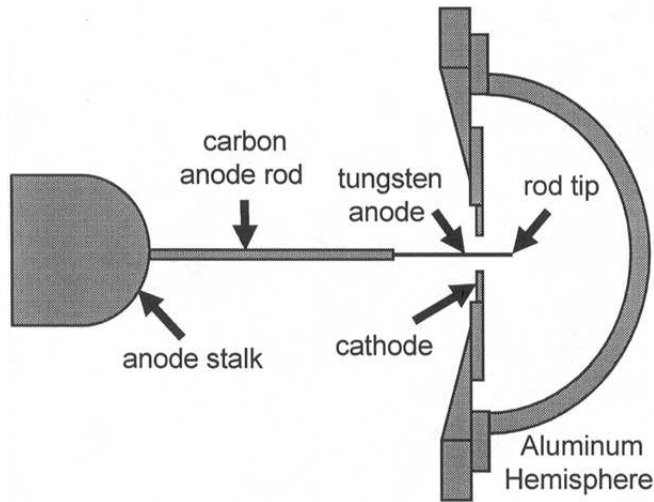


Figure 6: Rod-pinch experiments on the Asterix accelerator. The aluminum hemisphere has an inner radius of 100.0 mm and thickness 10.0 mm. (Courtesy S. Swanekamp.)

final parameters (species, position, kinetic energy, direction and current) for all model orbits. I loaded it into **GenDist**, set a filter to include only electrons with final position $r < 1.5$ mm and wrote an amended PRT file. I then performed a **GamBet** run to determine bremsstrahlung radiation from the tungsten anode tip with the following input components:

- A mesh to define the geometry of physical objects including the tungsten anode and the aluminum hemisphere. The intervening volume is a void. I included only the axial region $z < 0.0$ mm.
- The primary electrons created by **Trak** and recorded in the filtered PRT file.
- The field file generated by **Trak** giving the distribution of electric field and B_θ near the anode.

The primary and secondary electrons undergo material interactions while inside the tungsten anode and move under the influence of the electric and magnetic fields while in the void. The process is not entirely self-consistent because electrons transmitted through or scattered from the target do not contribute to the local space charge. On the other hand, they have relatively small effect on the intense electric fields near the rod. Figure 8 shows selected electron orbits and the dose-rate distribution near the rod tip. The deposited energy is strongly concentrated near the tip, implying a small effective source size. The source dimensions could also be determined by back-projecting

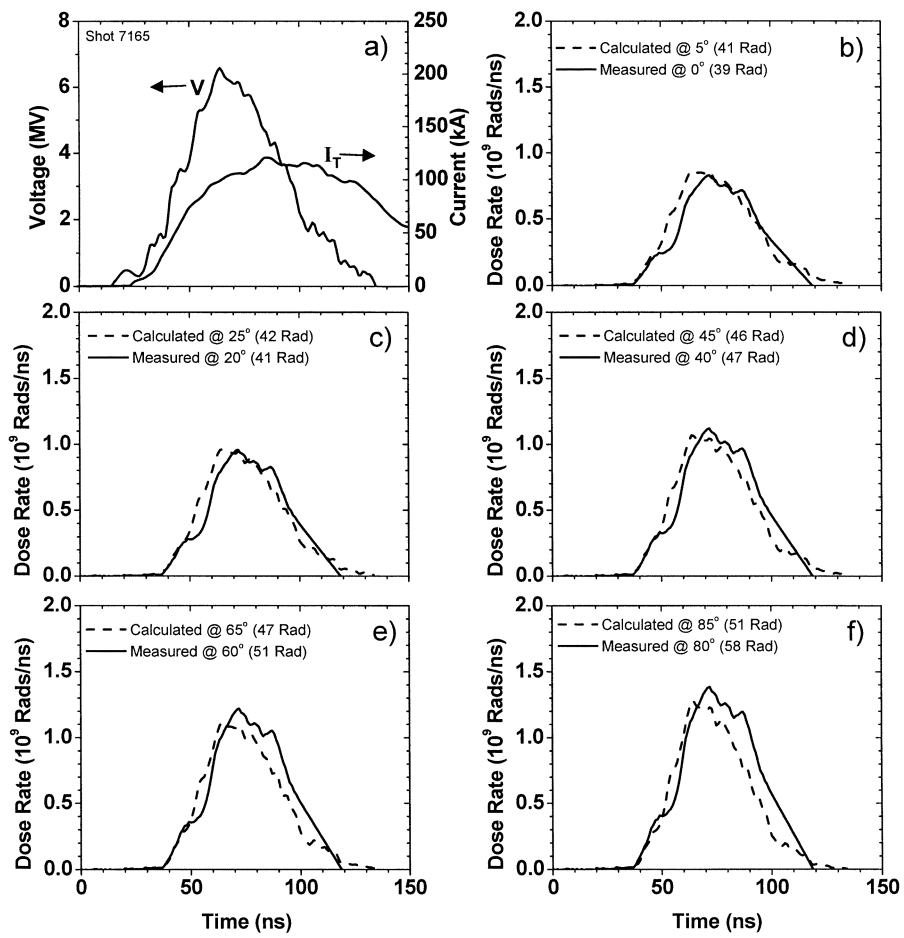


Figure 7: Measurements on the Asterix accelerator for the diode of Fig. 6. a) Current and voltage. b)-c) Measured dose rate at 1.0 m (solid line) with **LSP/ITS** predictions (dashed line) as a function of angle. (Courtesy, S. Swanekamp.)

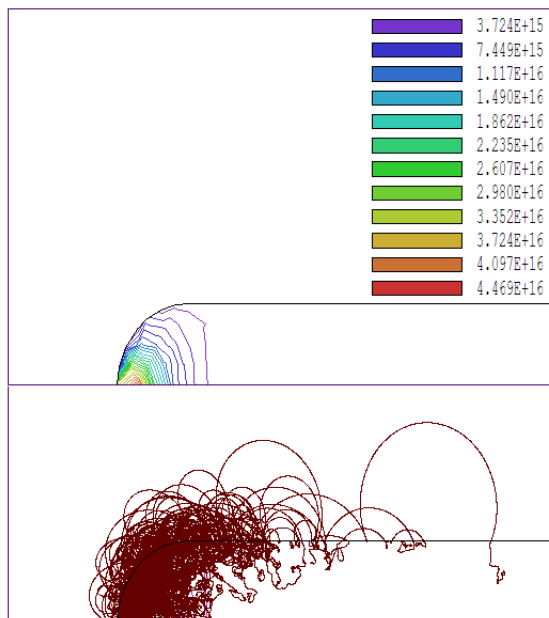


Figure 8: **GamBet** simulations of electron impact on the Asterix target. Top: Dose rate in Gy/s. Bottom: selected electron orbits. The tip radius is 1.0 mm.

bremsstrahlung photon orbits. The multiple electron transits through the target are evident in the plot, along with an $\mathbf{E} \times \mathbf{B}$ migration down the rod. Regarding particle balance, the code starts with 208 model electrons. The run has a primary multiplication factor $N_p = 10$, so that 2080 showers are initiated. Most of run time is occupied with orbit integrations of primary and secondary electrons in the void. A small spatial step is necessary for accurate representation of the highly convoluted orbits. A high value of the maximum cross-section energy is required in because a small number of positrons are accelerated across the gap with kinetic energy in the range 6-12 MeV.

The photons that escape the target cross the void and interact with the aluminum shell. The escape file contains photons (and possibly positrons) that pass through shell. With a bremsstrahlung forcing factor of 100.0, the escape file contains 229,103 photons. I filtered the escape file to remove the all positrons and photons with final positions $z \geq 0.0$ mm. The remaining photons were distributed in polar angle at spherical radius $R = 100.0$ mm.

The mesh of the second **GamBet** calculation contains a phantom, an aluminum hemisphere with inner radius 110.0 mm and outer radius 120.0 mm. The primary particles (the filtered photons from the previous run) are augmented by a factor $N_p = 100$ for good statistics. Figure 9 shows the calculated dose rate in the aluminum phantom. The anomaly near the axis is probably statistical because of the low number of particles per interval of

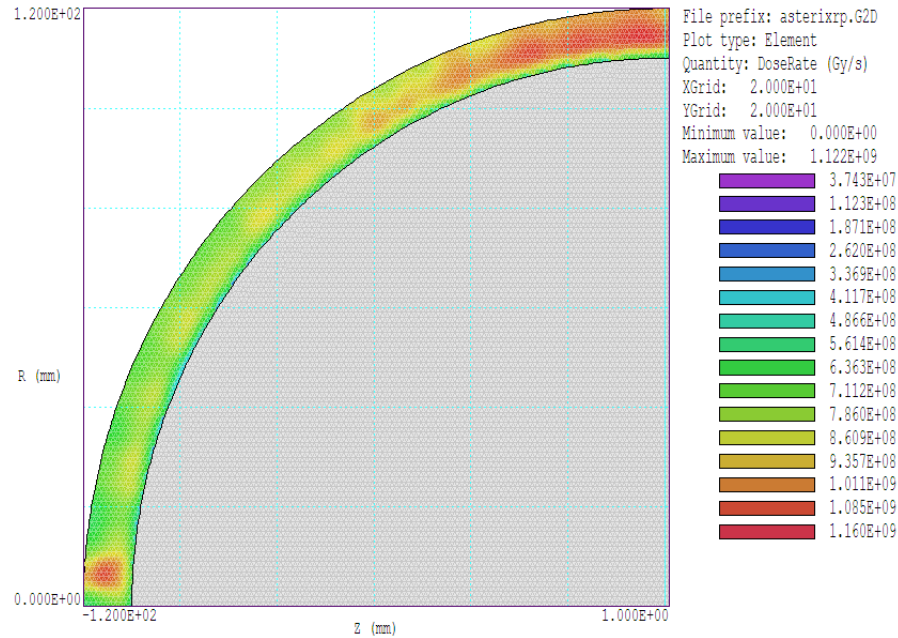


Figure 9: Dose-rate in an aluminum phantom, photon emission from the Asterix rod-pinch diode.

polar angle. The values in the figure are in Gy/s at an average radius of 0.115 m. Assuming inverse-square-law scaling, I multiplied by 1.32×10^{-9} to find the dose in rad/ns at 1.0 m. The results are 1.04 rad/ns at 5° and 1.52 rad/ns at 85° , in good agreement with values of Fig. 7

References

- [1] S. Swanekamp, *et.al.*, *Evaluation of self-magnetically-pinchd diodes up to 10 MV as high-resolution flash X-ray sources* (IEEE Trans. Plasma Sci. **32**, 2004), 2004.
- [2] F. Young, *et.al.* *Radiographic results for the rod-pinch diode scaled to 6 MV*, **Proc. Part. Acc. Conf** (IEEE, 0-7803-7915-2/03, Piscataway, 2003), 979.
- [3] S. Humphries and T. Orzechowski, *Simulation tools for pinched-electron-beam radiographic diodes*, Phys. Rev. Spec. Topics - Acc. and Beams **9**, (2006), 020401.